

xLSTM-SENet: xLSTM for Single-Channel Speech Enhancement

Nikolai Lund Kühne¹, Jan Østergaard¹, Jesper Jensen^{1,2}, Zheng-Hua Tan¹

¹Department of Electronic Systems, Aalborg University, Denmark

²Oticon A/S, Copenhagen, Denmark

{nlk, jo, jje, zt}@es.aau.dk

Abstract

While attention-based architectures, such as Conformers, excel in speech enhancement, they face challenges such as scalability with respect to input sequence length. In contrast, the recently proposed Extended Long Short-Term Memory (xLSTM) architecture offers linear scalability. However, xLSTM-based models remain unexplored for speech enhancement. This paper introduces xLSTM-SENet, the first xLSTM-based single-channel speech enhancement system. A comparative analysis reveals that xLSTM—and notably, even LSTM—can match or outperform state-of-the-art Mamba- and Conformer-based systems across various model sizes in speech enhancement on the VoiceBank+Demand dataset. Through ablation studies, we identify key architectural design choices such as exponential gating and bidirectionality contributing to its effectiveness. Our best xLSTM-based model, xLSTM-SENet2, outperforms state-of-the-art Mamba- and Conformer-based systems on the VoiceBank+DEMAND dataset.

Index Terms: xLSTM, speech enhancement, LSTM, Mamba

1. Introduction

Real-world speech signals are often disrupted by noise, which degrades performance in tasks such as hearing assistive devices [1], automatic speech recognition [2], and speaker verification [3]. The process of removing background noise and enhancing the quality and intelligibility of the desired speech signal is known as speech enhancement (SE). SE has a wide range of applications, which drives the development of new and improved algorithms.

Single-channel SE methods leveraging deep learning encompass a range of architectures, such as deep neural networks [1], recurrent Long Short-Term Memory (LSTM) networks [4], convolutional neural networks (CNNs) [5, 6], generative adversarial networks (GANs) [7–10], and diffusion models [11–13]. Recently, Conformer-based models have demonstrated impressive SE performance, achieving state-of-the-art results [10, 14] on the VoiceBank+Demand dataset [15, 16]. However, models based on scaled dot-product attention, such as Conformers, face challenges with scalability with respect to input sequence length, and require a lot of data to train [17].

However, recurrent neural networks (RNNs), particularly LSTMs [18], offer several advantages over attention-based models, including: (i) linear scalability, instead of quadratic, in terms of computational complexity with respect to the input sequence length, and (ii) reduced runtime memory requirements, as they do not require storage of the full key-value (KV) cache. In contrast, attention-based models such as Transformers and Conformers necessitate significant memory overhead for KV storage. Despite these advantages, LSTMs suffer from criti-

cal drawbacks: (i) inability to revise storage decisions, (ii) reliance on scalar cell states, constraining storage capacity, and (iii) memory mixing preventing parallelizability [19]. Consequently, LSTMs have been less utilized in recent deep learning-based SE systems, with only a few exceptions [4, 20].

To address the inherent limitations of attention-based models, Mamba [21], a sequence model integrating the strengths of CNNs, RNNs, and state space models, has recently emerged. Mamba has demonstrated competitive or superior performance relative to Transformers across various tasks, including audio classification [22] and SE [23]. Recently, the Extended Long Short-Term Memory architecture (xLSTM) [19] was proposed to overcome the limitations of LSTMs. By incorporating exponential gating, matrix memory, and improved normalization and stabilization mechanisms while eliminating traditional memory mixing, xLSTM introduces two new fundamental building blocks: sLSTM and mLSTM. The xLSTM architecture has shown competitive performance across tasks such as natural language processing [19], computer vision [24], and audio classification [25]. However, while xLSTM adds increased memory via matrix memory and an improved ability to revise storage decisions via exponential gating, the potential advantages of these additions over LSTM have yet to be assessed for SE.

In this work, we propose an xLSTM-based SE system (xLSTM-SENet), which is the first single-channel SE system utilizing xLSTM. The system architecture is illustrated in Figure 1. Systematic comparisons of our proposed xLSTM-SENet with Mamba-, and Conformer-based models across various model sizes, show that xLSTM-SENet matches the performance of state-of-the-art Mamba- and Conformer-based systems on the VoiceBank+Demand dataset [15, 16]. Intriguingly, we empirically show that LSTM matches or even outperforms xLSTM, Mamba, and Conformers on the VoiceBank+Demand dataset. Additionally, we perform detailed ablation studies to explore the design space of neural architectures, quantifying their impact on overall performance. Finally, our best xLSTM-based model, xLSTM-SENet2, outperforms state-of-the-art Mamba- and Conformer-based systems on the VoiceBank+DEMAND dataset. Code is publicly available.¹

2. Method

2.1. Extended long short-term memory

As mentioned, xLSTM [19] introduces two novel building blocks: sLSTM and mLSTM, to address the limitations of the original LSTM [18]. Following Vision-LSTM [24] and Audio xLSTM [25], we employ mLSTM as the main building block in our SE system. Unlike the sigmoid gating used in traditional

¹<https://github.com/NikolaiKyhne/xLSTM-SENet>

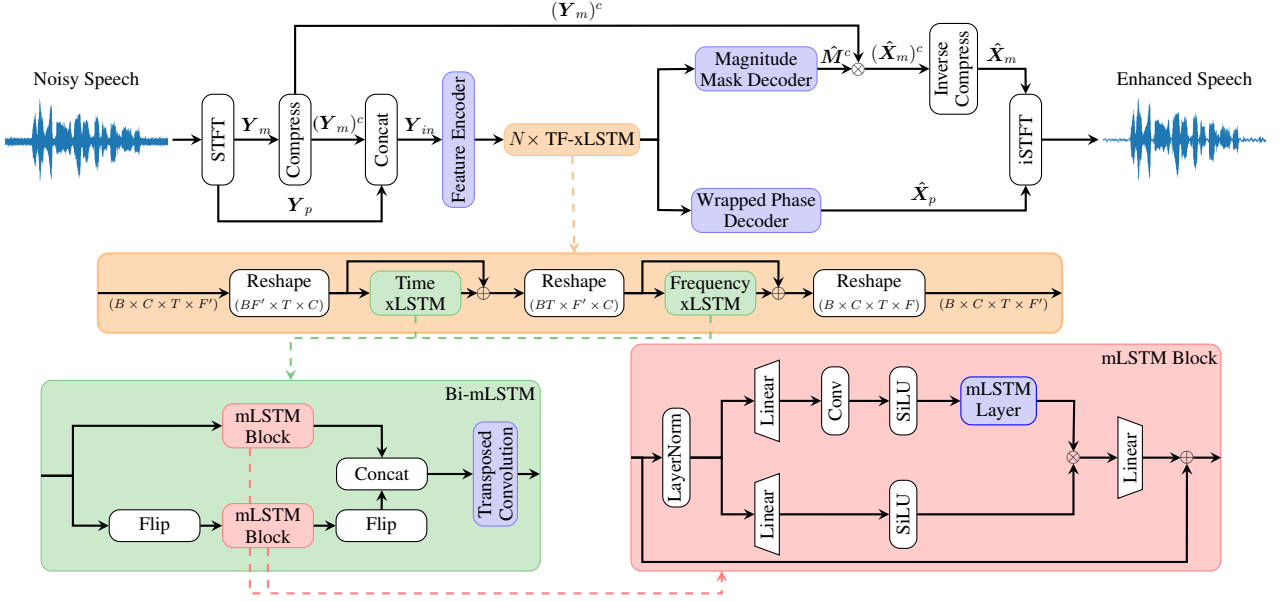


Figure 1: Overall structure of our proposed xLSTM-SENet with parallel magnitude and phase spectra denoising.

LSTMs, mLSTM adopts exponential gating for the input and forget gates, enabling it to better revise storage decisions. Additionally, the scalar memory cell $c \in \mathbb{R}$ is replaced with a matrix memory cell $\mathbf{C} \in \mathbb{R}^{d \times d}$ to increase storage capacity. Each mLSTM block projects the D -dimensional input by an expansion factor $E_f \in \mathbb{N}$ to $d = E_f D$ before projecting it back to D -dimensions after being processed by an mLSTM layer. The forward pass of mLSTM is given by [19]:

$$\mathbf{C}_t = f_t \mathbf{C}_{t-1} + i_t \mathbf{v}_t \mathbf{k}_t^\top, \quad (1)$$

$$\mathbf{n}_t = f_t \mathbf{n}_{t-1} + i_t \mathbf{k}_t, \quad (2)$$

$$\mathbf{h}_t = \mathbf{o}_t \odot \left(\mathbf{C}_t \mathbf{q}_t / \max \{ |\mathbf{n}_t^\top \mathbf{q}_t|, 1 \} \right), \quad (3)$$

$$\mathbf{q}_t = \mathbf{W}_q \mathbf{x}_t + \mathbf{b}_q, \quad (4)$$

$$\mathbf{k}_t = \frac{1}{\sqrt{d}} \mathbf{W}_k \mathbf{x}_t + \mathbf{b}_k, \quad (5)$$

$$\mathbf{v}_t = \mathbf{W}_v \mathbf{x}_t + \mathbf{b}_v, \quad (6)$$

$$i_t = \exp(\mathbf{w}_i^\top \mathbf{x}_t + b_i), \quad (7)$$

$$f_t = \exp(\mathbf{w}_f^\top \mathbf{x}_t + b_f), \quad (8)$$

$$\mathbf{o}_t = \sigma(\mathbf{W}_o \mathbf{x}_t + \mathbf{b}_o), \quad (9)$$

where the cell state $\mathbf{C}_t \in \mathbb{R}^{d \times d}$, $\mathbf{n}_t, \mathbf{h}_t \in \mathbb{R}^d$ represent the normalizer state and the hidden state, respectively, σ is the sigmoid function, and \odot is element-wise multiplication. The input, forget and output gates are represented by $i_t, f_t \in \mathbb{R}$ and $\mathbf{o}_t \in \mathbb{R}^d$, respectively, while $\mathbf{W}_q, \mathbf{W}_k, \mathbf{W}_v \in \mathbb{R}^{d \times d}$ are learnable projection matrices and $\mathbf{b}_q, \mathbf{b}_k, \mathbf{b}_v \in \mathbb{R}^d$ are the respective biases for the query, key and value vectors. Finally, $\mathbf{w}_i, \mathbf{w}_f \in \mathbb{R}^d$, and $\mathbf{W}_o \in \mathbb{R}^{d \times d}$ represent the weights between the input \mathbf{x}_t and the input, forget, and output gate, respectively, and $b_i, b_f \in \mathbb{R}$ and $\mathbf{b}_o \in \mathbb{R}^d$ are their biases. Unlike LSTM and sLSTM, there are no interactions between hidden states from one time step to the following in mLSTM (no memory mixing). This means multiple memory cells and multiple heads are equivalent, allowing the forward pass to be parallelized.

2.2. xLSTM-SENet: speech enhancement with xLSTMs

Following SEMamba [23], we integrate xLSTM into the MP-SENet architecture [14] by replacing the Conformers in MP-SENet with xLSTM blocks as shown in Figure 1. We use the MP-SENet architecture since it facilitates joint denoising of magnitude and phase spectra, and has shown superior performance compared to other time-frequency (TF) domain SE methods [14].

2.2.1. Model structure

Model overview: As shown in Figure 1, our proposed xLSTM-SENet architecture follows an encoder-decoder structure. Let T and F denote the time and frequency dimensions, respectively, and let $\mathbf{Y} = \mathbf{Y}_m \cdot e^{j\mathbf{Y}_p} \in \mathbb{C}^{T \times F}$ denote the complex spectrogram, which is obtained by performing a STFT on the noisy speech waveform $\mathbf{y} \in \mathbb{R}^D$. Then $\mathbf{Y}_p \in \mathbb{R}^{T \times F}$ is the wrapped phase spectrum, and by applying power-law compression [26] with compression factor $0 < c \in \mathbb{R}$, we extract the compressed magnitude spectrum $(\mathbf{Y}_m)^c \in \mathbb{R}^{T \times F}$. The stacked compressed magnitude spectrum and wrapped phase spectrum $\mathbf{Y}_{in} = (\mathbf{Y}_m)^c \oplus \mathbf{Y}_p \in \mathbb{R}^{T \times F \times 2}$, where \oplus is the concatenation operator, is encoded into a compressed TF-domain representation, which is subsequently fed to a stack of N TF-xLSTM blocks. Each TF-xLSTM block comprises a time and frequency xLSTM block, capturing temporal and frequency dependencies, respectively. Similar to SEMamba [23], we use a bidirectional architecture (Bi-mLSTM) for these blocks. Hence, the output \mathbf{v} of the time and frequency xLSTM blocks is:

$$\mathbf{v} = \text{Conv1D}(\text{mLSTM}(\boldsymbol{\varepsilon}) \oplus \text{mLSTM}(\text{flip}(\boldsymbol{\varepsilon}))), \quad (10)$$

where $\boldsymbol{\varepsilon}$ is the input to the time and frequency xLSTM blocks, and $\text{mLSTM}(\cdot)$, $\text{flip}(\cdot)$, and $\text{Conv1D}(\cdot)$ is the unidirectional mLSTM, the sequence flipping operation, and the 1-D transposed convolution, respectively.

Finally, the output of the TF-xLSTM blocks is decoded by both a magnitude mask decoder and wrapped phase decoder [27]. They predict the clean compressed magnitude mask

$M^c = (\mathbf{X}_m/\mathbf{Y}_m)^c \in \mathbb{R}^{T \times F}$ and the clean wrapped phase spectrum $\hat{\mathbf{X}}_p \in \mathbb{R}^{T \times F}$, respectively. The enhanced magnitude spectrum $\hat{\mathbf{X}}_m \in \mathbb{R}^{T \times F}$ is obtained by computing:

$$\hat{\mathbf{X}}_m = ((\mathbf{Y}_m)^c \odot \hat{M}^c)^{1/c}, \quad (11)$$

where \hat{M}^c is the predicted clean compressed magnitude mask. The final enhanced waveform $\hat{\mathbf{x}}$ is reconstructed by performing an iSTFT on the enhanced magnitude spectrum $\hat{\mathbf{X}}_m$ and the enhanced wrapped phase spectrum $\hat{\mathbf{X}}_p$.

Similar to MP-SENet and SEMamba, we use a linear combination of loss functions which includes a PESQ-based GAN discriminator, time, magnitude, complex, and phase losses as in [14]. We also employ the consistency loss function proposed in [28], as this has been shown to improve performance [23].

Feature encoder: Following MP-SENet [14], the encoder consists of two convolution blocks each comprising a 2D convolutional layer, an instance normalization, and parametric rectified linear unit (PReLU) activation, sandwiching a dilated DenseNet [29] with dilation sizes 1, 2, 4, and 8. The first convolutional block increases the input channels from 2 to C , while the second convolutional block halves the frequency dimension from F to $F' = F/2$, consequently reducing the computational complexity in the TF-xLSTM blocks. The dilated DenseNet extends the receptive field along the time axis, which facilitates long-range context aggregation over different resolutions.

Magnitude mask and phase decoder: Following MP-SENet [14], both the magnitude mask decoder and the phase decoder consist of a dilated DenseNet and a 2D transposed convolution. For the magnitude mask decoder, this is followed by a deconvolution block reducing the output channel number C to 1. To estimate the magnitude mask, we employ a learnable sigmoid function with $\beta = 2$ as in [9]. In the phase decoder, the transposed convolution is followed by two parallel 2D convolutional layers outputting the pseudo-real and pseudo-imaginary part components. To predict the clean wrapped phase spectrum, we use the two-argument arctangent (Arctan2) function resulting in the enhanced wrapped phase spectrum $\hat{\mathbf{X}}_p$.

3. Experiments

3.1. Dataset

In this study, we perform experiments on the VoiceBank+Demand dataset, which consists of pairs of clean and noisy audio clips sampled at 48 kHz. The clean audio samples come from the VoiceBank corpus [15], which comprises 11,572 audio clips from 28 distinct speakers for training, and 824 audio clips from 2 distinct speakers for testing. The noisy audio clips are created by mixing the clean samples with noise from the DEMAND dataset [16] at four signal-to-noise ratios (SNRs) during training ([0, 5, 10, 15] dB) and testing ([2.5, 7.5, 12.5, 17.5] dB). Two speakers from the training set are left out as a validation set.

3.2. Implementation details

Unless otherwise stated, experimental details and training configurations match those presented in MP-SENet [14] and SEMamba [23]. To reduce memory and computational resources, all models were trained on randomly cropped 2-second audio clips. Additionally, all audio clips were downsampled to 16 kHz, reducing computational complexity and ensuring compatibility with the wide-band PESQ metric [30]. When performing STFTs we set the FFT order, Hann window size, and

hop size to 400, 400, and 100, respectively. We train all models for 200 epochs and select the checkpoint (saved every 1000th step) with the best PESQ score on the validation data. We fix $C = 64$ channels and $N = 4$ stacks of TF-xLSTM blocks in our xLSTM-SENet model for direct comparison with SEMamba and MP-SENet. All models are trained with a batch-size $B = 8$ on four NVIDIA L40S GPUs, and the four layer xLSTM-SENet model takes approximately 3 days to train. This is the main limitation of xLSTM compared to Mamba and Transformers, which are roughly four times as fast to train [19].

3.3. Evaluation metrics

We use the following commonly used evaluation metrics to assess SE performance: wide-band PESQ [30] and short-time objective intelligibility (STOI) [31]. To predict the signal distortion, background intrusiveness and overall speech quality, we use the composite measures CSIG, CBAK and COVL [32]. For all measures, a higher value is better. We train all models with 5 different seeds and document the mean and standard deviation.

4. Results and analysis

4.1. Comparison with existing methods

We evaluate several architectural design choices for our xLSTM-SENet model while limiting the parameter count to that of SEMamba. We choose the best model based on validation performance. Our best model uses a bidirectional architecture and we have added biases to layer normalizations and projection layers as in [24]. The expansion factor is set to $E_f = 4$.

Table 1: *Results on the VoiceBank+Demand dataset. “-” denotes the result is not provided in the original paper. * means the results are reproduced using the original provided code.*

Model	Params (M)	PESQ	CSIG	CBAK	COVL	STOI
Noisy	-	1.97	3.35	2.44	2.63	0.91
MetricGAN+ [9]	-	3.15	4.14	3.16	3.64	-
CMGAN [10]	1.83	3.41	4.63	3.94	4.12	0.96
DPT-FSNet [33]	0.88	3.33	4.58	3.72	4.00	0.96
Spiking-S4 [34]	0.53	3.39	4.92	2.64	4.31	-
TridentSE [35]	3.03	3.47	4.70	3.81	4.10	0.96
MP-SENet [14]	2.05	3.50	4.73	3.95	4.22	0.96
SEMamba [23]	2.25	3.55	4.77	3.95	4.29	0.96
MP-SENet*	2.05	3.49±0.02	4.72±0.02	3.92±0.04	4.22±0.02	0.96±0.00
SEMamba*	2.25	3.49±0.01	4.75±0.01	3.94±0.02	4.24±0.01	0.96±0.00
xLSTM-SENet	2.20	3.48±0.00	4.74±0.01	3.93±0.01	4.22±0.01	0.96±0.00

Table 1 shows that xLSTM-SENet matches the performance of the state-of-the-art SEMamba and MP-SENet models on the VoiceBank+Demand dataset, while outperforming other SE methods on most metrics. This demonstrates the effectiveness of xLSTM for SE.

4.2. Ablation study

mLSTM adds matrix memory and exponential gating to improve LSTM. To evaluate some of these improvements and our model architecture design choices, we perform ablations on the expansion factor E_f and on the biases in layer normalizations and projection layers. Additionally, we evaluate the effect of exponential gating by replacing it with sigmoid gating. Finally, we investigate the performance of a unidirectional architecture, by removing the transposed convolution, flipping and the second

mLSTM block within each time and frequency xLSTM block as shown in Figure 1, while doubling the amount of layers N to match the parameter count of xLSTM-SENet.

Table 2: Ablation study on the VoiceBank+Demand dataset. Default settings for xLSTM-SENet: $E_f = 4$, a bidirectional architecture, and biases in layer normalizations and projection layers.

Model	Params (M)	PESQ	CSIG	CBAK	COVL	STOI
Noisy	-	1.97	3.35	2.44	2.63	0.91
xLSTM-SENet	2.20	3.48±0.00	4.74±0.01	3.93±0.01	4.22±0.01	0.96±0.00
$E_f = 3$	1.96	3.46±0.01	4.72±0.00	3.93±0.02	4.21±0.01	0.96±0.00
$E_f = 2$	1.71	3.45±0.01	4.71±0.01	3.92±0.01	4.19±0.01	0.96±0.00
w/o Biases	2.18	3.46±0.00	4.72±0.01	3.91±0.01	4.20±0.02	0.96±0.00
w/o Exp. gating	2.20	3.45±0.02	4.72±0.02	3.90±0.01	4.20±0.03	0.96±0.00
Unidirectional	2.14	3.26±0.02	4.57±0.02	3.79±0.01	4.00±0.02	0.95±0.00

Table 2 shows that decreasing the expansion factor E_f decreases performance. Moreover, as in Vision-LSTM [24], biases in layer normalizations and projection layers improve performance. We also find that a bidirectional architecture significantly outperforms a unidirectional architecture. Finally, we find that exponential gating slightly improves performance for SE, which was not the case for learning self-supervised audio representations with xLSTMs [25].

4.3. Comparison with LSTM

To compare the performance of xLSTM and LSTM for SE, we first replace the mLSTM layers in xLSTM-SENet with conventional LSTM layers (this model is referred to as: LSTM (layer)). Table 3 shows that this results in a performance decrease even though LSTM (layer) is approximately 11% larger. Then, we replace the entire mLSTM block with LSTM (denoted as: LSTM (block)) and double the number of layers N to match the parameter count of xLSTM-SENet. Table 3 shows that LSTM (block) matches xLSTM-SENet, which in Table 1 was shown to match the enhancement performance of state-of-the-art Mamba and Conformer-based systems.

Table 3: Comparison of xLSTM with LSTM on the VoiceBank+Demand dataset.

Model	Params (M)	PESQ	CSIG	CBAK	COVL	STOI
Noisy	-	1.97	3.35	2.44	2.63	0.91
xLSTM-SENet	2.20	3.48±0.00	4.74±0.01	3.93±0.01	4.22±0.01	0.96±0.00
LSTM (layer)	2.44	3.44±0.01	4.69±0.02	3.90±0.00	4.17±0.01	0.96±0.00
LSTM (block)	2.34	3.49±0.02	4.76±0.01	3.95±0.01	4.24±0.01	0.96±0.00

4.4. Scaling experiments

Smaller models are preferred in real-world SE applications, like hearing aids, due to reduced computational complexity, facilitating their use in such devices. Additionally, it is of interest to explore the performance achieved by increasing model sizes. Hence, we perform a comparative analysis of xLSTM, Mamba, Conformer and LSTM across varying layer counts N . For LSTM, N is doubled to match the parameter counts of the xLSTM-, Mamba-, and Conformer-based models.

Figure 2 shows that xLSTM, Mamba, and Conformer-based models perform similarly when scaled down, with LSTM out-

performing them for $N = 1$ and $N = 2$. When scaled up, all models achieve comparable performance.

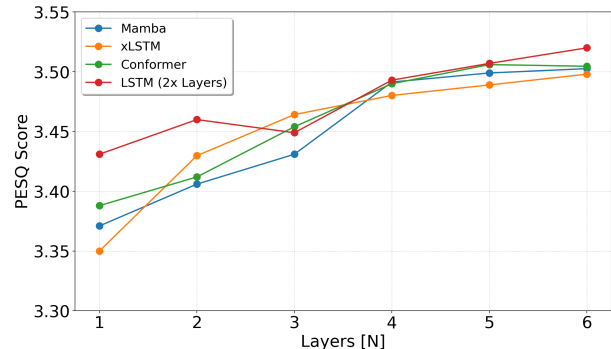


Figure 2: Scaling results on the VoiceBank+Demand dataset. The smallest ($N = 1$) and largest ($N = 6$) models are 1.37 M and 2.94 M parameters, respectively.

4.5. xLSTM-SENet2

To provide a direct comparison of xLSTM and LSTM for SE, we propose xLSTM-SENet2, which is configured with an expansion factor $E_f = 2$ and $N = 8$ layers, resulting in approximately the same parameter count per layer for xLSTM-SENet2 and LSTM (block). Table 4 shows that xLSTM-SENet2 outperforms state-of-the-art LSTM-, Mamba-, and Conformer-based models.

Table 4: Speech enhancement performance of xLSTM-SENet2 on the VoiceBank+Demand dataset. * means the results are reproduced using the original provided code.

Model	Params (M)	PESQ	CSIG	CBAK	COVL	STOI
Noisy	-	1.97	3.35	2.44	2.63	0.91
LSTM (block)	2.34	3.49±0.02	4.76±0.01	3.95±0.01	4.24±0.01	0.96±0.00
MP-SENet*	2.05	3.49±0.02	4.72±0.02	3.92±0.04	4.22±0.02	0.96±0.00
SEMamba*	2.25	3.49±0.01	4.75±0.01	3.94±0.02	4.24±0.01	0.96±0.00
xLSTM-SENet2	2.27	3.53±0.01	4.78±0.01	3.98±0.02	4.27±0.01	0.96±0.00

5. Conclusion

This paper proposed an Extended Long Short-Term Memory-based method for speech enhancement (xLSTM-SENet). Experiments on the VoiceBank+Demand dataset show that xLSTM-SENet, and even LSTM-based models, rival existing state-of-the-art Mamba- and Conformer-based speech enhancement systems across several model sizes. We studied the importance of several architectural design choices, and demonstrated that the inclusion of exponential gating and bidirectionality is critical to the performance of the xLSTM-SENet model. Finally, empirical results show that our best xLSTM-based system, xLSTM-SENet2, outperforms state-of-the-art systems in speech enhancement on the VoiceBank+Demand dataset.

6. References

- [1] M. Kolbæk, Z.-H. Tan, and J. Jensen, "Speech intelligibility potential of general and specialized deep neural network based speech enhancement systems," *IEEE/ACM Transactions on Au-*

- dio, *Speech, and Language Processing*, vol. 25, no. 1, pp. 153–167, 2016.
- [2] Z. Chen, S. Watanabe, H. Erdogan, and J. R. Hershey, “Speech enhancement and recognition using multi-task learning of long short-term memory recurrent neural networks,” in *INTER-SPEECH*, 2015, pp. 3274–3278.
 - [3] S. Shon, H. Tang, and J. Glass, “Voiceid loss: Speech enhancement for speaker verification,” in *INTERSPEECH*, 2019, pp. 2888–2892.
 - [4] K. Tesch, N.-H. Mohrmann, and T. Gerkmann, “On the role of spatial, spectral, and temporal processing for dnn-based non-linear multi-channel speech enhancement,” in *INTERSPEECH*, 2022, pp. 2908–2912.
 - [5] S.-W. Fu, Y. Tsao, X. Lu *et al.*, “Snr-aware convolutional neural network modeling for speech enhancement,” in *INTERSPEECH*, 2016, pp. 3768–3772.
 - [6] M. Kolbæk, Z.-H. Tan, S. H. Jensen, and J. Jensen, “On loss functions for supervised monaural time-domain speech enhancement,” *IEEE/ACM Transactions on Audio, Speech, and Language Processing*, vol. 28, pp. 825–838, 2020.
 - [7] D. Michelsanti and Z.-H. Tan, “Conditional generative adversarial networks for speech enhancement and noise-robust speaker verification,” in *INTERSPEECH*, 2017, pp. 2008–2012.
 - [8] S.-W. Fu, C.-F. Liao, Y. Tsao, and S.-D. Lin, “Metricgan: Generative adversarial networks based black-box metric scores optimization for speech enhancement,” in *International Conference on Machine Learning*. PmlR, 2019, pp. 2031–2041.
 - [9] S.-W. Fu, C. Yu, T.-A. Hsieh, P. Plantinga, M. Ravanelli, X. Lu, and Y. Tsao, “Metricgan+: An improved version of metricgan for speech enhancement,” in *INTERSPEECH*, 2021, pp. 201–205.
 - [10] S. Abdulatif, R. Cao, and B. Yang, “Cmgan: Conformer-based metric-gan for monaural speech enhancement,” *IEEE/ACM Transactions on Audio, Speech, and Language Processing*, 2024.
 - [11] Y.-J. Lu, Z.-Q. Wang, S. Watanabe, A. Richard, C. Yu, and Y. Tsao, “Conditional diffusion probabilistic model for speech enhancement,” in *IEEE International Conference on Acoustics, Speech and Signal Processing (ICASSP)*. IEEE, 2022, pp. 7402–7406.
 - [12] J. Richter, S. Welker, J.-M. Lemercier, B. Lay, and T. Gerkmann, “Speech enhancement and dereverberation with diffusion-based generative models,” *IEEE/ACM Transactions on Audio, Speech, and Language Processing*, vol. 31, pp. 2351–2364, 2023.
 - [13] P. Gonzalez, Z.-H. Tan, J. Østergaard, J. Jensen, T. S. Alstrøm, and T. May, “Investigating the design space of diffusion models for speech enhancement,” *IEEE/ACM Transactions on Audio, Speech, and Language Processing*, 2024.
 - [14] Y.-X. Lu, Y. Ai, and Z.-H. Ling, “Mp-senet: A speech enhancement model with parallel denoising of magnitude and phase spectra,” in *INTERSPEECH*, 2023, pp. 3834–3838.
 - [15] C. Veaux, J. Yamagishi, and S. King, “The voice bank corpus: Design, collection and data analysis of a large regional accent speech database,” in *2013 international conference oriental COCOSDA held jointly with 2013 conference on Asian spoken language research and evaluation (O-COCOSDA/CASLRE)*. IEEE, 2013, pp. 1–4.
 - [16] J. Thiemann, N. Ito, and E. Vincent, “The diverse environments multi-channel acoustic noise database (demand): A database of multichannel environmental noise recordings,” in *Proceedings of Meetings on Acoustics*, vol. 19, no. 1. AIP Publishing, 2013.
 - [17] Y. Gong, Y.-A. Chung, and J. Glass, “Ast: Audio spectrogram transformer,” in *INTERSPEECH*, 2021, pp. 571–575.
 - [18] J. Schmidhuber, S. Hochreiter *et al.*, “Long short-term memory,” *Neural Computation*, vol. 9, no. 8, pp. 1735–1780, 1997.
 - [19] M. Beck, K. Pöppel, M. Spanring, A. Auer, O. Prudnikova, M. K. Kopp, G. Klambauer, J. Brandstetter, and S. Hochreiter, “xL-STM: Extended long short-term memory,” in *The Thirty-eighth Annual Conference on Neural Information Processing Systems (NeurIPS)*, 2024.
 - [20] K. Tesch and T. Gerkmann, “Multi-channel speech separation using spatially selective deep non-linear filters,” *IEEE/ACM Transactions on Audio, Speech, and Language Processing*, vol. 32, pp. 542–553, 2023.
 - [21] A. Gu and T. Dao, “Mamba: Linear-time sequence modeling with selective state spaces,” in *First Conference on Language Modeling (COLM)*, 2024.
 - [22] S. Yadav and Z.-H. Tan, “Audio mamba: Selective state spaces for self-supervised audio representations,” in *INTERSPEECH*, 2024, pp. 552–556.
 - [23] R. Chao, W.-H. Cheng, M. La Quatra, S. M. Siniscalchi, C.-H. H. Yang, S.-W. Fu, and Y. Tsao, “An investigation of incorporating mamba for speech enhancement,” in *IEEE Spoken Language Technology Workshop*, 2024.
 - [24] B. Alkin, M. Beck, K. Pöppel, S. Hochreiter, and J. Brandstetter, “Vision-lstm: xlstm as generic vision backbone,” *arXiv preprint arXiv:2406.04303*, 2024.
 - [25] S. Yadav, S. Theodoridis, and Z.-H. Tan, “Audio xlstms: Learning self-supervised audio representations with xlstms,” *arXiv preprint arXiv:2408.16568*, 2024.
 - [26] S. Wisdom, J. R. Hershey, K. Wilson, J. Thorpe, M. Chinen, B. Patton, and R. A. Saurous, “Differentiable consistency constraints for improved deep speech enhancement,” in *IEEE International Conference on Acoustics, Speech and Signal Processing (ICASSP)*, 2019, pp. 900–904.
 - [27] Y. Ai and Z.-H. Ling, “Neural speech phase prediction based on parallel estimation architecture and anti-wrapping losses,” in *IEEE International Conference on Acoustics, Speech and Signal Processing (ICASSP)*. IEEE, 2023, pp. 1–5.
 - [28] V. Zadorozhnyy, Q. Ye, and K. Koishida, “Sep-gan: Self-correcting discriminator optimization for training consistency preserving metric gan on speech enhancement tasks,” in *INTERSPEECH*, 2023, pp. 2463–2467.
 - [29] A. Pandey and D. Wang, “Densely connected neural network with dilated convolutions for real-time speech enhancement in the time domain,” in *IEEE International Conference on Acoustics, Speech and Signal Processing (ICASSP)*, 2020, pp. 6629–6633.
 - [30] A. W. Rix, J. G. Beerends, M. P. Hollier, and A. P. Hekstra, “Perceptual evaluation of speech quality (pesq)-a new method for speech quality assessment of telephone networks and codecs,” in *2001 IEEE international conference on acoustics, speech, and signal processing. Proceedings (Cat. No. 01CH37221)*, vol. 2. IEEE, 2001, pp. 749–752.
 - [31] C. H. Taal, R. C. Hendriks, R. Heusdens, and J. Jensen, “An algorithm for intelligibility prediction of time-frequency weighted noisy speech,” *IEEE Transactions on audio, speech, and language processing*, vol. 19, no. 7, pp. 2125–2136, 2011.
 - [32] Y. Hu and P. C. Loizou, “Evaluation of objective quality measures for speech enhancement,” *IEEE Transactions on audio, speech, and language processing*, vol. 16, no. 1, pp. 229–238, 2007.
 - [33] F. Dang, H. Chen, and P. Zhang, “Dpt-fsnet: Dual-path transformer based full-band and sub-band fusion network for speech enhancement,” in *IEEE International Conference on Acoustics, Speech and Signal Processing (ICASSP)*. IEEE, 2022, pp. 6857–6861.
 - [34] Y. Du, X. Liu, and Y. Chua, “Spiking structured state space model for monaural speech enhancement,” in *IEEE International Conference on Acoustics, Speech and Signal Processing (ICASSP)*. IEEE, 2024, pp. 766–770.
 - [35] D. Yin, Z. Zhao, C. Tang, Z. Xiong, and C. Luo, “Tridentse: Guiding speech enhancement with 32 global tokens,” in *INTERSPEECH*, 2023, pp. 3839–3843.